



Deposited via The University of Leeds.

White Rose Research Online URL for this paper:

<https://eprints.whiterose.ac.uk/id/eprint/140860/>

Version: Accepted Version

Article:

Litschko, C, Brühmann, S, Csiszár, A et al. (2019) Functional integrity of the contractile actin cortex is safeguarded by multiple Diaphanous-related formins. *Proceedings of the National Academy of Sciences of the United States of America*, 116 (9). pp. 3594-3603. ISSN: 0027-8424

<https://doi.org/10.1073/pnas.1821638116>

© 2019, Published under the PNAS license. This is an author produced version of a paper published in *Proceedings of the National Academy of Sciences of the United States of America*. Uploaded in accordance with the publisher's self-archiving policy.

Reuse

Items deposited in White Rose Research Online are protected by copyright, with all rights reserved unless indicated otherwise. They may be downloaded and/or printed for private study, or other acts as permitted by national copyright laws. The publisher or other rights holders may allow further reproduction and re-use of the full text version. This is indicated by the licence information on the White Rose Research Online record for the item.

Takedown

If you consider content in White Rose Research Online to be in breach of UK law, please notify us by emailing eprints@whiterose.ac.uk including the URL of the record and the reason for the withdrawal request.

Functional integrity of the contractile actin cortex is safeguarded by multiple Diaphanous-related formins

Christof Litschko¹, Stefan Brühmann¹, Agnes Csiszár², Till Stephan¹, Vanessa Dimchev³, Julia Damiano-Guercio¹, Alexander Junemann¹, Sarah Körber¹, Moritz Winterhoff¹, Benjamin Nordholz¹, Nagendran Ramalingam⁴, Michelle Peckham⁵, Klemens Rottner³, Rudolf Merkel², Jan Faix¹

¹Hannover Medical School, ²Forschungszentrum Jülich GmbH, ³Technische Universität Braunschweig, ⁴Harvard Medical School, ⁵University of Leeds

Submitted to Proceedings of the National Academy of Sciences of the United States of America

The contractile actin cortex is a thin layer of filamentous actin, myosin motors and regulatory proteins beneath the plasma membrane crucial to cytokinesis, morphogenesis and cell migration. However, the factors regulating actin assembly in this compartment are not well understood. Using the *Dictyostelium* model system, we show that the three Diaphanous-related formins (DRFs) ForA, ForE and ForH are regulated by the RhoA-like GTPase RacE and synergize in the assembly of filaments in the actin cortex. Single or double formin-null mutants displayed only moderate defects in cortex function whereas the concurrent elimination of all three formins or of RacE caused massive defects in cortical rigidity and architecture as assessed by aspiration assays and electron microscopy. Consistently, the triple formin- and RacE-mutants encompassed large peripheral patches devoid of cortical F-actin and exhibited severe defects in cytokinesis and multicellular development. Unexpectedly, many *forA*/*H/E* and *racE*-mutants protruded efficiently, formed multiple exaggerated fronts and migrated with morphologies reminiscent of rapidly-moving fish keratocytes. In 2D-confinement, however, these mutants failed to properly polarize and recruit myosin II to the cell rear essential for migration. Cells arrested in these conditions displayed dramatically amplified flow of cortical actin filaments, as revealed by TIRF-imaging and iterative particle image velocimetry (PIV). Consistently, individual and combined, CRISPR/Cas9-mediated disruption of genes encoding mDia1 and -3 formins in B16-F1 mouse melanoma cells revealed enhanced frequency of cells displaying multiple fronts, again accompanied by defects in cell polarization and migration. These results suggest evolutionarily conserved functions for formin-mediated actin assembly in actin cortex mechanics.

actin cortex | formin | RhoGTPase | cell migration | cytokinesis

Introduction

The actin-rich cell cortex is required for cell shape remodeling in fundamental cellular processes such as cytokinesis, morphogenesis and cell migration (1). Cell motility is regulated by polarization, adhesion and cytoskeletal activities leading to site-specific force generation, as exemplified by leading edge actin assembly and myosin-dependent rear contraction (2–4). Based on considerable variations of these activities in different cell types, this process is further subdivided into mesenchymal and amoeboid types of migration as two extremes of a wide spectrum (5). The slow mesenchymal type of motility is characterized by strong substrate adhesion and formation of prominent stress fibers as well as a protruding lamellipodium at the front (6), whereas fast amoeboid migration as exemplified by *Dictyostelium* cells is defined by weaker and more transient adhesions, a rounder cell shape, actin-rich protrusions or blebs in the front and myosin-driven contraction in the rear (7, 8). However, migration and other processes involving cell shape remodeling as e.g. cytokinesis also require a thin, actin-rich cortex below the membrane.

This cortex contains actin, myosin and associated factors assembling into a multi-component layer (9, 10), which is intimately linked to the membrane in a PI(4,5)P₂-dependent manner by the

ezrin, radixin and moesin (ERM)-family of proteins in animal cells (11, 12) and cortexillin (Ctx) in *Dictyostelium* (13–15). The function of this thin actin meshwork is comparable to cell walls in plants, yeast and bacteria, as it defines the cell's stiffness, resists external forces and counteracts intracellular, hydrostatic pressure (9, 16). However, as opposed to the static cell wall of plants and bacteria, the actin cortex of amoebae and animal cells has viscoelastic properties that can be remodeled in the timescale of seconds. Rapid F-actin rearrangements enable cells to promptly modify their shapes for fast adaptation to changes in extracellular environment (9, 16). Moreover, and as opposed to cells with rigid cell walls engaging them entirely, cell cortex constituents of motile eukaryotic cells are organized in gradients due to the asymmetry of positioning signals (17).

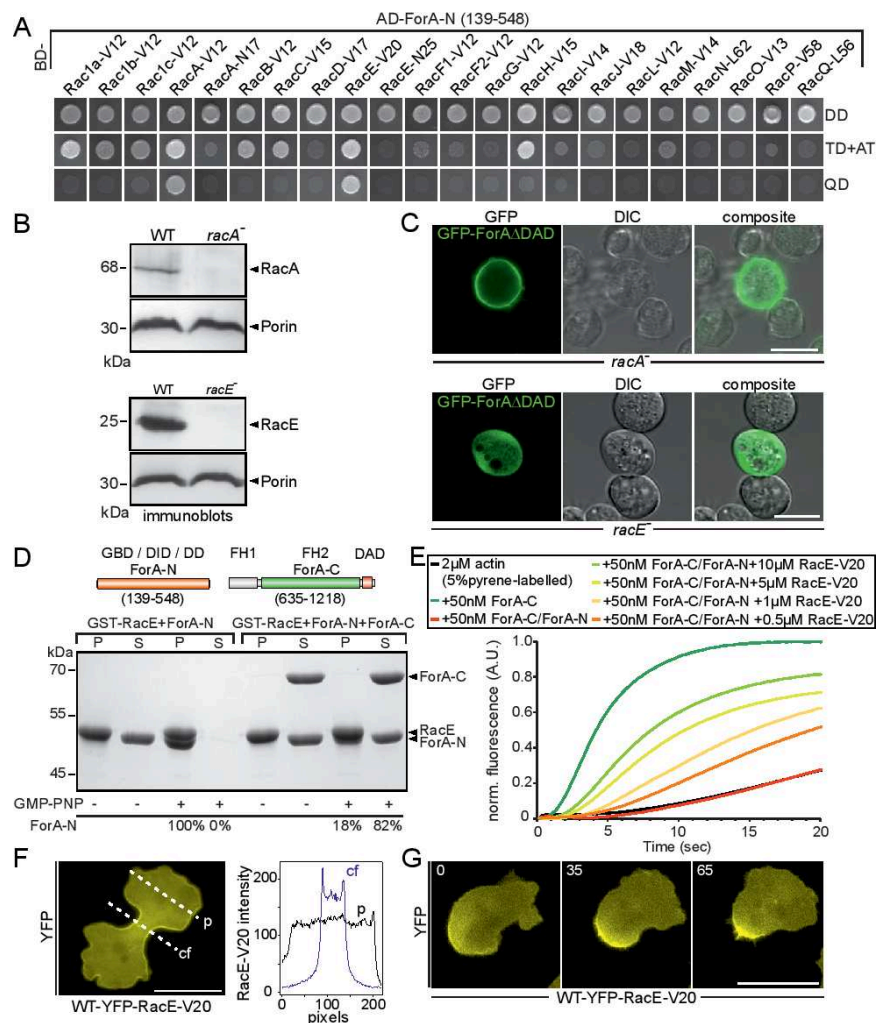
The physical properties of the cell cortex such as its tension and contractility likely impacting on plasma membrane dynamics are regulated by myosin motor activity as well as the arrangement and density of F-actin networks generated by distinct actin-assembly machineries (9). In cells, actin polymerization is mostly initiated by Arp2/3 complex and formins (18). The Arp2/3 complex creates branches at the sides of preexisting mother filaments and generates a dense actin meshwork at the front of migrating cells (18, 19). Formins instead nucleate and elongate long and linear actin filaments (19). A major subgroup of the formin family is comprised by Diaphanous-related formins (DRFs), which are autoinhibited due to intramolecular interactions of the Diaphanous

Significance

The actin-rich cell cortex is a viscoelastic structure participating in a variety of cellular processes. However, the complete inventory of actin assembly factors driving its formation and knowledge about their specific contributions is still incomplete. We show here that functional integrity of the cell cortex in *Dictyostelium* and mammalian cells is backed up by multiple Diaphanous-related formins that are regulated by Rho-subfamily GTPases. These DRFs contribute to the generation of long actin filaments of the contractile actin cortex and are required for cell mechanics. Of note, these factors are excluded from Arp2/3 complex-nucleated networks, implying diversification of the cortex into functional subcompartments to segregate cortical actomyosin contraction in the rear or cleavage furrow ingression from actin-based protrusion in the front.

Reserved for Publication Footnotes

137
138
139
140
141
142
143
144
145
146
147
148
149
150
151
152
153
154
155
156
157
158
159
160
161
162
163
164
165
166
167
168
169
170
171
172
173
174
175
176
177
178
179
180
181
182
183
184
185
186
187
188
189
190
191
192
193
194
195
196
197
198
199
200
201
202
203
204



205
206
207
208
209
210
211
212
213
214
215
216
217
218
219
220
221
222
223
224
225
226
227
228
229
230
231
232
233
234
235
236
237
238
239
240
241
242
243
244
245
246
247
248
249
250
251
252
253
254
255
256
257
258
259
260
261
262
263
264
265
266
267
268
269
270
271
272

Fig. 1. ForA is regulated by the RhoA-homologue RacE. (A) The N-terminal domain of ForA (ForA-N) containing the GBD interacts specifically with the activated forms of RacA (RacA-V12) and RacE (RacE-V20) in the Y2H assay. Yeast was transformed with the indicated constructs and selected for the presence of prey and bait plasmids by growth on double-dropout (DD) media lacking leucine and tryptophan. Interactions were assayed by growth on stringent triple-dropout (TD) media additionally lacking histidine in the presence of 3 mM 3-AT and on quadruple-dropout (QD) media additional lacking histidine and adenine. AD, Gal4-activation domain; 3-AT, 3-amino-1,2,4-triazole; (B) Genetic elimination of RacA and RacE was confirmed by immunoblotting. Porin was used as a loading control. (C) Constitutively active ForA fused to GFP requires RacE for targeting to the cell cortex but localizes appropriately in the absence of RacA. Scale bars, 10 μ m. (D) ForA constructs used for biochemical analyses. GBD, GTPase-binding domain; DID, diaphanous inhibitory domain; DD, dimerization domain; FH, formin homology domain; DAD, diaphanous autoinhibitory domain. Active RacE interacts directly with ForA-N and was able to partially release ForA-N from the autoinhibited ForA-N/ForA-C complex. GST-pulldown experiments with GMPPNP-loaded RacE are shown. (P) pellet; (S) supernatant. The numbers below indicate the relative amounts of ForA-N in P and S fractions. (E) Active RacE releases autoinhibition of the catalytically inactive ForA-N/ForA-C complex to promote actin assembly in pyrene assays in a concentration-dependent manner. (F) Active RacE N-terminally fused to YFP accumulates about 2-fold in the cell cortex of the cleavage furrow in 2D-confinement under agar. Abbreviations: cf, cleavage furrow; p, pole. Scale bar, 20 μ m. (G) Images from lime-lapse movies correspond to Movie S1 and show that active RacE is enriched in the rear cell cortex of a polarized cell migrating under agar. Scale bar, 20 μ m.

inhibitory domain (DID) with the Diaphanous autoregulatory domain (DAD) (20). DRF autoinhibition is commonly released by binding of activated Rho-family GTPases (21, 22), but can also be driven by Ras (23). As yet, both Arp2/3 complex and formins have been implicated in the generation of cortical actin in different cell types (24, 25). However, the precise quantitative contributions of Arp2/3 complex- and formin- generated filaments to this structure and their interplay in cortical functions are still elusive. Depletion of the formin mDia1 (Diaph1) in HeLa cells led to failure of cortex function in mitotic cell division, while depletion of Arp2/3 complex alone did not (24). Interestingly, the same study reported Arp2/3 complex inhibition to potentiate effects of mDia1 depletion, suggesting synergistic activities of mDia1 and Arp2/3 complex in the nucleation of cortical actin (24). AFM measurements indicated that cortical elasticity in HeLa and M2

melanoma cells is mostly affected by the formin inhibitor SmiFH2 (25). In contrast, reducing Arp2/3 complex activity by CK666 did not appear to play a critical role (25). These data suggested central roles for formins in cell cortex mechanics, but need to be complemented by genetics, last not least to identify specific, contributing formins.

Previously, we established that the mDia1-related formin ForA in *Dictyostelium* cells prevents blebbing in the rear to assist protrusion at the front, in particular under mechanical stress (18). Here, we identify and characterize two additional mDia-related, cortical *Dictyostelium* formins, ForE and ForH, which synergize with ForA to safeguard cortex-dependent functions. Moreover, we extend our studies to mammalian formins mDia1 and -3, providing conclusive evidence that comparable pathways operate in higher eukaryotes.

273
274
275
276
277
278
279
280
281
282
283
284
285
286
287
288
289
290
291
292
293
294
295
296
297
298
299
300
301
302
303
304
305
306
307
308
309
310
311
312
313
314
315
316
317
318
319
320
321
322
323
324
325
326
327
328
329
330
331
332
333
334
335
336
337
338
339
340

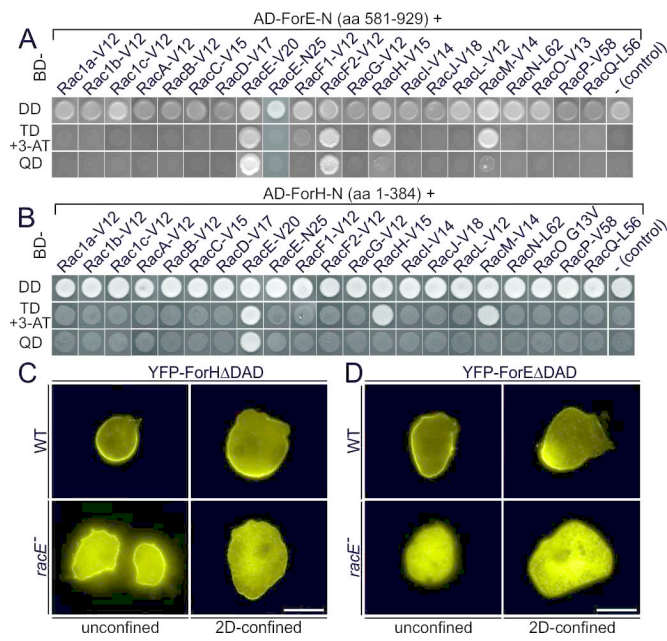


Fig. 2. Active RacE interacts with two additional cortical formins. (A-B) ForE-N and ForH-N interact specifically with the active form of RacE (V20) in the Y2H assay. Yeast was transformed with the indicated constructs and selected for the presence of prey and bait plasmids by growth on double-dropout (DD) media lacking leucine and tryptophan. ForE-N additionally showed strong interaction with active RacF2 (V12). Interactions were scored by growth on stringent triple-dropout (TD) media in the presence of 3 mM 3-AT or quadruple-dropout (QD) media as outlined in Fig. 2. Both formins showed no genetic interaction using the dominant-negative RacE (N25) variant or empty AD plasmids as negative controls. AD, Gal4-activation domain; 3-AT, 3-amino-1,2,4-triazole; BD, Gal4-binding domain. (C-D) Constitutively active ForE and ForH localize in the cell cortex and rear of migrating WT cells. YFP-tagged variants of the formins were expressed in WT and *racE* cells and analyzed by wide-field fluorescence microscopy at the conditions indicated. Scale bars, 10 μ m.

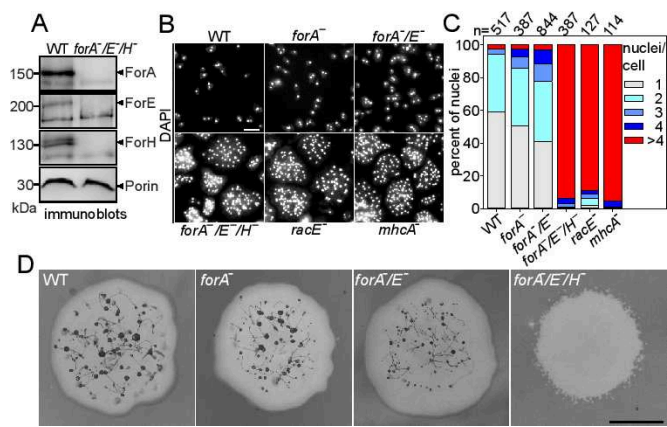


Fig. 3. Elimination of all three cortical formins is detrimental for cell division and development. (A) Inactivation of the *forA*, *forE* and *forH* genes in the triple knockout mutant was verified by immunoblotting using specific formin sera. Porin was used as a loading control. (B) WT and the mutant cells indicated were grown for 48 h in shaken suspension at 150 rpm, subsequently seeded on glass cover slips, fixed and stained with DAPI to visualize the nuclei. Scale bar, 20 μ m. (C) Quantification of nuclei in cells as shown in (B). n, number of analyzed cells. (D) Coincident elimination of ForA, ForE and ForH blocks development. WT or formin-deficient cells were transferred with a tooth pick onto a lawn of *K. aerogenes* on non-nutrient agar plates and monitored after 96-120 h of development. Scale bar, 0.5 mm.

Results

Active ForA accumulates in the cleavage furrow of dividing cells. Consistent with the mechanistic similarities between migration and cytokinesis, many proteins accumulating in the trailing edge, as for instance myosin II, cortaxillin (Ctx), the functional homologue of ERM proteins in *Dictyostelium*, and IQGAPs, were also found in cleavage furrows and are known to regulate cytokinesis (26–28). Thus, we explored the localization of active ForA at different stages of the cell cycle. Active ForA is uniformly localized in the cell cortex of unpolarized interphase cells (17). In mitotic cells, active ForA remained evenly distributed in the cell cortex up to early anaphase, but subsequently began to relocalize to the cleavage furrow like IQGAP1 and Ctx I ("SI Appendix, Fig. S1 A and B"), strongly suggesting a critical function of formin-generated cortical actin in cytokinesis, as previously shown in a variety of cell types (29). However, when cultivated in petri dishes allowing adhesion of cells to the substratum, or even when exposed to high shear forces in shaken suspension culture, *forA* cells exhibited negligible defects in cytokinesis ("SI Appendix Fig. S1 C and D"). Of note, we have previously shown that either Ctx I and II or IQGAP1 and IQGAP2 had to be eliminated simultaneously to cause strong defects in cytokinesis, while single knockout mutants exhibited no or minor defects (28). Thus, the lack of a cytokinesis defect in *forA* cells suggested functional overlaps of ForA with one or multiple other cortical formins to safeguard this critical cellular function. In line with this view, cortical F-actin is still present in contractile regions of *forA* cells, such as the trailing edge (17).

ForA interacts with active form of the RhoA homologue RacE. DRFs such as ForA are commonly assumed to be activated by GTP-bound Rho-family GTPases. *Dictyostelium* cells lack canonical Cdc42 and Rho homologues, but express 20 Rac proteins, some of which exert characteristics of Cdc42 and RhoA functions. Since appropriate ForA targeting and activation requires concurrent interactions with PI(4,5)P2 and an active GTPase (17), we employed yeast-two-hybrid (Y2H) analyses to systematically screen all 20 *Dictyostelium* Racs for interaction with the N-terminal domain of ForA encompassing the GBD. Under the most stringent growth conditions on selective media, ForA genetically interacted with constitutively active RacA and RacE, while it failed to interact with dominant-negative variants of these GTPases (Fig. 1A). RacA has not yet been characterized, but contains a BTB domain at its C-terminus and lacks a classical CAAX motive required for prenylation (30). Consistently, ectopically expressed RacA fused to GFP localized ubiquitously in the cytoplasm and was not enriched at the cell cortex (Fig. S2). Thus, it appeared unlikely that it regulates recruitment and activation of ForA at the cortex. RacE instead was previously implicated in regulation of cortical tension and cleavage furrow progression (31). Since Y2H analyses can occasionally generate ambiguous results, we sought to corroborate these findings in an independent assay. To this end, we generated genetic knockout cell lines devoid of RacA and RacE in the AX2 wild type (WT) strain (Fig. 1B). Then, we monitored localization of constitutively active ForA fused to GFP in these knockouts. As shown in Fig. 1C, ForA was normally targeted to the cell cortex in *racA*⁻ cells, but failed to localize to the cortex in *racE*⁻ cells, strongly suggesting a physiological interaction between ForA and RacE. Consistently, the purified N-terminus of ForA also physically interacted with GMP-PNP-loaded RacE in pull-down experiments (Fig. 1D). In addition, constitutively active RacE was capable to release autoinhibition of an inactive formin sandwich complex formed by N- and C-terminal fragments of ForA in both pulldowns and pyrene assays (Fig. 1D and E). Finally, we monitored localization of active RacE fused to YFP in cells in 2D-confinement, i.e. under a thin sheet of agar. Unlike previous work that failed to detect active RacE in the cleavage furrow of unconfined cells (32), the active

341
342
343
344
345
346
347
348
349
350
351
352
353
354
355
356
357
358
359
360
361
362
363
364
365
366
367
368
369
370
371
372
373
374
375
376
377
378
379
380
381
382
383
384
385
386
387
388
389
390
391
392
393
394
395
396
397
398
399
400
401
402
403
404
405
406
407
408

409
410
411
412
413
414
415
416
417
418
420
421
422
423
424
425
426
427
428
429
430
431
432
433
434
435
436
437
438
439
440
441
442
443
444
445
446
447
448
449
450
451
452
453
454
455
456
457
458
459
460
461
462
463
464
465
466
467
468
469
470
471
472
473
474
475
476

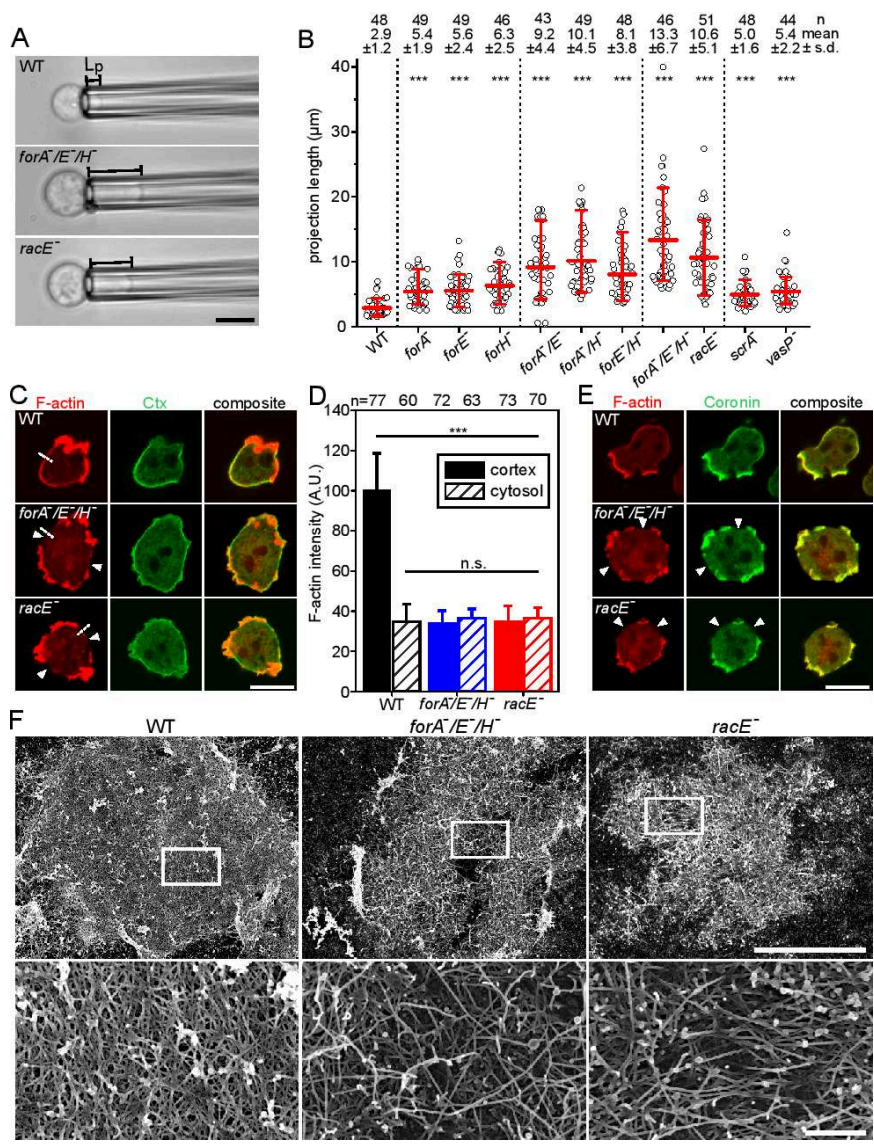


Fig. 4. Elimination of the three cortical formins or of RacE increasingly impairs cortical rigidity and disrupts the contractile actin cortex. (A) Projection length (Lp) of WT and the mutant cells indicated was determined by micropipette aspiration using a constant suction pressure of 500 Pa from time-lapse movies and correspond to Movie S2. Scale bar, 10 µm. (B) Quantitative analysis of the projection lengths of probed cells. n, number of analyzed cells, ***P < 0.001 by Mann-Whitney rank sum test. Statistical differences refer to WT. (C) Defects of the actin cortex in *forA/E/H* and *racE* mutants. Fixed WT and mutant cells were stained with a monoclonal Ctx antibody (green) to visualize PI(4,5)P2-containing membranes and F-actin with phalloidin (red). The white arrow heads indicate regions of low cortical density in the mutants. Scale bar, 10 µm. (D) Quantification of cortical and intracellular actin in WT and mutant cells. Average intensity profiles along 5 pixel wide lines as shown in (C) by the white dashed lines. n, number of analyzed cells; error bars, standard deviations (s.d.). (E) Prominent cortical F-actin assemblies outside the breaches in *forA/E/H* and *racE* cells are identified as protrusions through containing coronin (green), particularly marking Arp2/3 complex-driven actin networks, and phalloidin-stained F-actin (red). Scale bar, 10 µm. (F) Representative SEM micrographs of detergent-extracted WT and mutant cells (low magnification and high magnification of insets shown at top and bottom, respectively). Scale bars, 5 µm (overview) and 0.5 µm (insets).

GTPase accumulated about two-fold in the cleavage furrow as compared to pole regions upon 2D-confinement (Fig. 1F). Moreover, like active ForA, the GTPase was also markedly enriched in the rear cortex of migrating cells (Fig. 1G and ("SI Appendix, Movie S1")), substantiating the view that ForA is regulated by RacE.

Active RacE additionally interacts with cortical formins ForE and ForH. Based on the critical effect of RacE deficiency on cytokinesis, contractility and the regulation of ForA, and the fact that ForE constitutes the only known Rho-family GTPase in *Dictyostelium* with RhoA-like functions, we reasoned that additional formins may interact with the active GTPase and localize to the cell cortex to safeguard cortex functions. Thus, from the 10 formins expressed in *Dictyostelium* cells (33), we screened all four potential candidates expressed at the vegetative stage, referred to as ForB, ForE (dDia3), ForH (dDia2) and ForF (dDia1) with Rho- GTPases in the Y2H assay. ForI could be excluded from the screen because of lacking the regulatory GBD, and ForG was omitted due to its specific interaction with active Ras (23).. Strong and specific interactions with active RacE were identified for two of the four tested formins. ForE interacted with active variants of RacE and RacF2 (Fig. 2A). However, since RacF2 appears

to carry out specific functions in macrocyst formation during the sexual cycle (34), we did not follow that lead. Unexpectedly, active RacE also interacted with ForH (Fig. 2B), previously shown to operate in filopodia formation (35).

Next, we examined the subcellular localization of constitutively active ForE and ForH variants lacking the DAD regions and fused to YFP in freely moving or 2D-confined WT and *racE* cells. Consistent with previous work (35), ectopic expression of active ForH in WT cells triggered the formation of numerous filopodia, with the active formin being markedly enriched at the cell cortex and filopodial tips (Fig. 2C and ("SI Appendix, Fig. S3")). In 2D-confinement, filopodia formation was strongly suppressed and active ForH accumulated in the rear cortex of migrating cells, resembling localization of active ForA under the same conditions (17). To our surprise, and as opposed to the entirely diffuse localization of active ForA in *racE* cells, constitutively active ForH was still able to trigger filopodia formation and accumulate in the cell cortex of freely moving *racE* mutant cells. In 2D-confinement, however, the formin became largely cytosolic and failed to be incorporated into the rear.

Active ForE also markedly localized to the cortex of unconfined WT cells and to distal tips of filopodia (Fig. 2D and Fig.

477
478
479
480
481
482
483
484
485
486
487
488
489
490
491
492
493
494
495
496
497
498
499
500
501
502
503
504
505
506
507
508
509
510
511
512
513
514
515
516
517
518
519
520
521
522
523
524
525
526
527
528
529
530
531
532
533
534
535
536
537
538
539
540
541
542
543
544

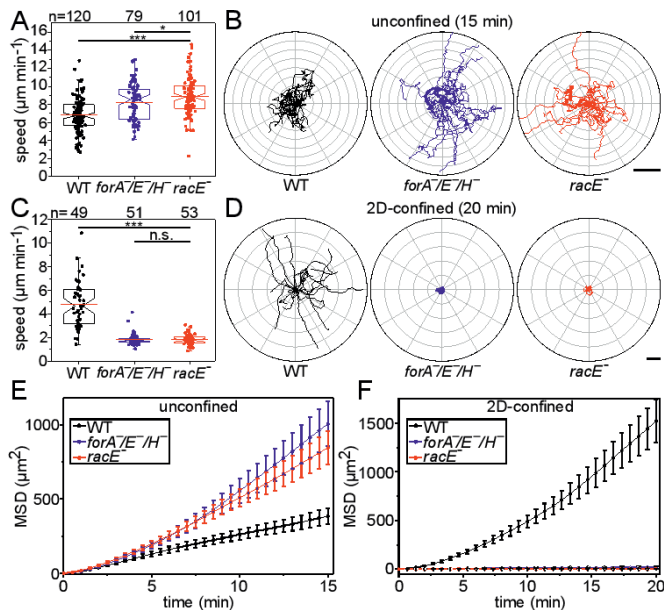


Fig. 5. *ForA/E/H* and *racE* mutants cannot migrate in 2D-confinement. (A and C) Box plots summarizing the random migration speed of WT, *ForA/E/H* and *racE* cells in (A) unconfined and (C) 2D-confined conditions. At least three movies from three independent experiments were analyzed for each cell type. n, number of cells analyzed. n.s. non-significant, * $p < 0.05$, *** $p < 0.001$ by Mann-Whitney rank sum test. (B and D) Radar plots showing the trajectories of 20 randomly migrating WT, *ForA/E/H* and *racE* cells in unconfined and 2D-confined conditions as indicated. Note the high directional persistence of the mutant cells in unconfined settings. Scale bars, 30 μm for (B) and 20 μm for (D). (E and F) Analysis of the mean square displacement of WT, *ForA/E/H* and *racE* cells migrating in unconfined and 2D-confined conditions as indicated. Error bars represent s.e.m. n as in (A) and (C).

S3). In the *racE* mutant, however, the formin was not targeted to the cortex and remained diffuse in the cytoplasm under both experimental settings, implying a requirement for RacE signaling to mediate appropriate subcellular targeting. Consistently, and as previously shown for RacE (36), active ForA, ForH and ForE localized in folate gradients after treatment with latrunculin B specifically on that portion of the plasma membrane facing lower chemoattractant concentrations ("SI Appendix, Fig. S4"). Thus, *Dictyostelium* cells express three RacE-regulated formins that accumulate in cell cortex and rear of cells migrating in 2D-confinement.

Elimination of the three cortical formins causes drastic cytokinesis and developmental defects. To uncover a potential functional redundancy of these three RacE-regulated, cortical formins, we eliminated them all either alone or in combination by gene disruption, to obtain a complete collection of single- and double-mutants as well as a cell line lacking all three formins (Fig. 3A and ("SI Appendix, Fig. S5")). Mutant lines devoid of either ForA or ForH have previously been described (17, 35). Next, we asked whether, or to which extent, cytokinesis is impaired after consecutive elimination of these cortical formins. For that, we first assayed cytokinesis of the *forA*-single, the *forA/E*-double and the *forA/E/H*-triple mutant at high stringency in shaken suspension, and compared effects obtained with RacE- and myosin II-null mutants known to exhibit strong defects in mitotic cell division under these conditions (37, 38). After fixing the cells together with DAPI, we quantified number of nuclei per cell as an unambiguous readout for cytokinesis defects. In cells harvested from shaken suspension after 48 h, the vast majority of WT cells, *forA*-single, and *forA/E*-double mutants was mono- or bi-nucleated, although a few *forA/E*-double mutant cells also displayed three

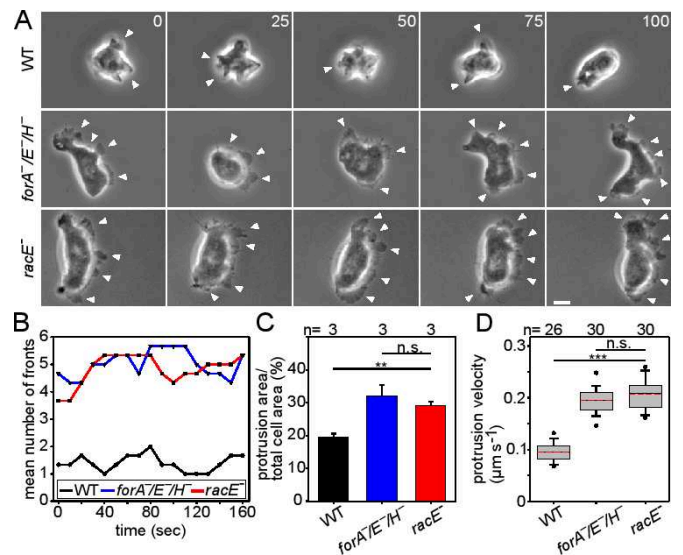


Fig. 6. *ForA/E/H* and *racE* mutants form multiple and faster protruding fronts. (A) Gallery with stills from a phase-contrast time-lapse series of randomly migrating WT and mutant cells in unconfined settings corresponding to Movie S4 shows the recurring formation of multiple fronts (white arrow heads) in *ForA/E/H* and *racE* mutants. Time is in seconds. Scale bar, 5 μm . (B) Quantification of the average number of protruding fronts in migrating WT and mutant cells as shown in (A). (C) Quantification of the ratio of protrusion area over total cell area in WT and indicated mutant cells. Error bars represent s.e.m. n.s. non-significant, ** $p < 0.01$ by Mann-Whitney rank sum test. (D) Average protrusion velocities of fronts in WT and mutant cells. Boxes include 50% and whiskers 80% of all measurements, dots represent the 5th/95th percentile. n, number of cells analyzed. n.s. non-significant, *** $p < 0.001$ by Mann-Whitney rank sum test.

or four nuclei (Fig. 3 B and C). By contrast, the *forA/E/H*-triple mutant exhibited a severe cytokinesis defect and was virtually indistinguishable from *racE* and *mhcA* mutants, since about 90% of these mutants developed highly multinucleated cells (Fig. 3 B and C). To exclude the possibility that a specific formin executes a predominant function in cytokinesis, we additionally performed these cytokinesis assays with all three combinations of double-mutant cells. Although mutant cell lines lacking ForH had a stronger tendency to form multinucleated cells, about 80% of all three formin double-null mutants still contained cells with only one or two nuclei ("SI Appendix, Fig. S6"). Thus, a severe cytokinesis defect was only manifested after inactivation of all three cortical formins.

Importantly, multicellular development also depends on contractility and cortical integrity. Myosin II mutants for instance cannot advance beyond the aggregation stage (39) and double mutants devoid of Ctx I/Ctx II known to tether cortical actin filaments to the membrane entirely fail to develop (40). Thus, we additionally compared multicellular development of WT cells, *forA*-single, *forA/E*-double, and the *forA/E/H*-triple mutant on bacterial lawns. Similar to WT, single- and double formin mutants were still able to advance through development and produce viable spores, although fruiting bodies of the *forA/E*-double mutant already appeared considerably smaller (Fig. 4D). Notably, the *forA/E/H*-triple mutant was completely blocked in development and not even able to aggregate. Thus, consistent with their overlapping functions in cytokinesis, all three formins have to be eliminated simultaneously to abrogate morphogenesis.

ForA, ForE and ForH synergize in the maintenance of cortical integrity. To quantify the assumed synergistic role of these formins in cortical integrity in the absence of adhesion forces, and to directly compare their contributions to this with those of *racE*, we performed micropipette aspiration assays (MPA)

681
682
683
684
685
686
687
688
689
690
691
692
693
694
695
696
697
698
699
700
701
702
703
704
705
706
707
708
709
710
711
712
713
714
715
716
717
718
719
720
721
722
723
724
725
726
727
728
729
730
731
732
733
734
735
736
737
738
739
740
741
742
743
744
745
746
747
748

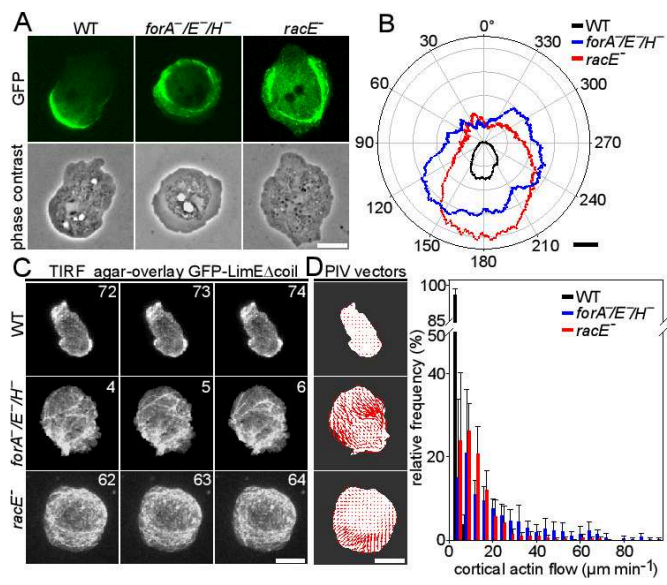


Fig. 7. *ForA/E/H* and *racE* mutants cannot polarize and exhibit a drastically increased cortical flow in 2D-confinement. (A) The characteristic localization of GFP-myosin II in the rear cortex of WT cells is abolished in *forA/E/H* and *racE* mutant cells illustrating a major defect in polarization. Still images from time-lapse movies correspond to Movie S6. Scale bar, 10 μ m. (B) Quantification of the width of the cortical myosin layer in WT and mutant cells determined by rotational analysis of the fluorescence signal from cells as shown in (A). Radar plot shows the mean myosin II band thickness of the cell lines indicated. Scale bar, 0.5 μ m. (C) Still images from TIRF time-lapse movies of WT and mutant cells expressing the F-actin probe GFP-LimE Δ coil in 2D-confined conditions under agar. Time is in seconds. Scale bar, 10 μ m. (D) PIV analyses of cortical actin flow in WT and mutant cells. Five consecutive frames recorded at 0.5 s intervals corresponding to Movie S7 were used for PIV analysis. The resulting vectors mark the mean actin velocity per frame (left). Distribution of actin flow velocities of the cell lines indicated reveal a strikingly increased actin flow in the mutants (right). Error bars are s.e.m..

of resuspended WT and mutant cells to measure their global mechanical resistance. To avoid secondary responses of the highly dynamic *Dictyostelium* cells to external suction pressure, we quantified the initial projection length (L_p) of cells captured from suspension at a constant pressure of 500 Pa in MPA assays. Serial elimination of the formins correlated with increasing defects of cortical rigidity and peaked in the *forA/E/H*-triple mutant with an average indentation length of $13 \pm 6.7 \mu$ m (mean \pm s.d.) as opposed to $3 \pm 1.2 \mu$ m in WT cells (Fig. 4 A and B). In contrast to many WT cells, *forA/E/H* cells were unable to withdraw from the micropipette even at this comparably low suction pressure, and all of them were ultimately sucked into the pipette within 5-10 min ("SI Appendix, Movie S2"). *RacE* cells also exhibited a major defect of cortical rigidity with an L_p of $11 \pm 5.1 \mu$ m, although the defect was slightly weaker as compared to the formin triple-knockout mutant. Unexpectedly, however, and albeit none of the analyzed cells was able to completely withdraw from the pipette, almost all cells (98%) resisted complete aspiration at 500 Pa within 10 min. Finally, we also measured the cortical properties of mutant cells lacking the Arp2/3-complex activator Scar and the actin filament elongator VASP. Cortex rigidity of *scrA* and *vasP* cells was also clearly impaired as compared to control. However, the contribution of Scar and of VASP was moderate, since measured L_p values were only in the range of the formin single-knockout mutants. Thus, in *Dictyostelium* Arp2/3 complex and VASP appear to contribute far less to mechanical rigidity of the cortex as compared to formins.

Next, we examined the distribution of cortical F-actin in fixed WT, *forA/E/H* and *racE* cells after phalloidin staining. Additionally, we labelled the specimens for PI(4,5)P₂-binding Ctx, to

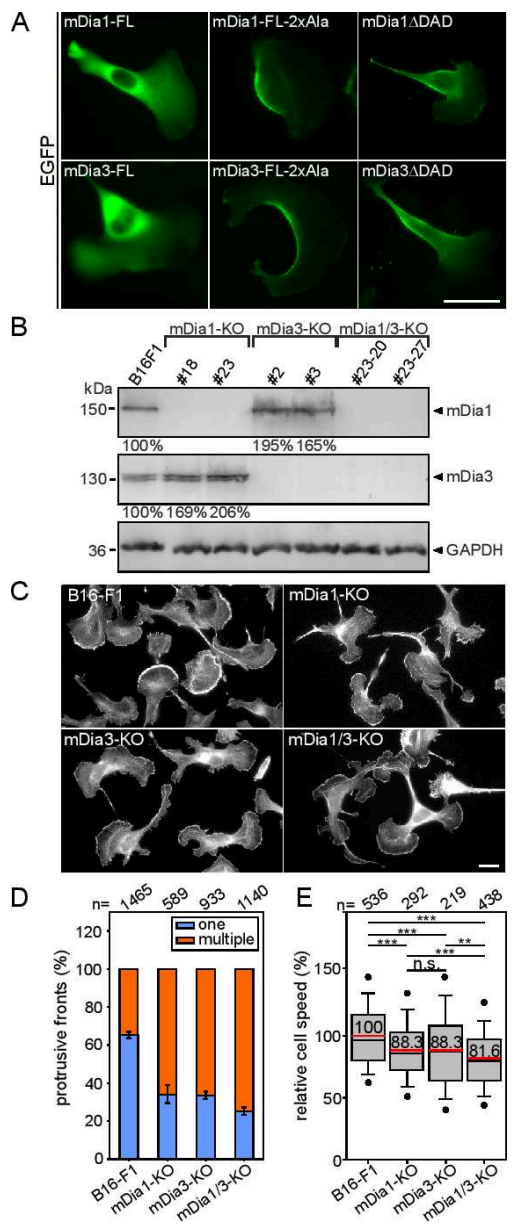


Fig. 8. Formation of multiple fronts and defects in polarization and migration in mDia1- and/or -3-deficient B16-F1 cells. (A) Subcellular localization of EGFP-mDia1 and -3 variants in B16-F1 cells migrating on laminin. While full-length (FL) mDia1 and -3 were cytosolic and largely excluded from protrusive fronts, constitutively active mDia1-FL-2xAla (M1182A and F1195A), mDia1 Δ DAD, mDia3-FL-2xAla (M1057A and F1170A) and mDia3 Δ DAD strongly accumulated in the rear cortex. Scale bar, 20 μ m. (B) Immunoblotting of individual and combined mDia1 and mDia3 KO clones as indicated, GAPDH: loading control. Numbers below respective lanes indicate relative changes of mDia1 and -3 expression levels normalized to GAPDH. (C) Polarization defects and formation of multiple fronts in respective cell types, as revealed by phalloidin-staining. Note increasingly pronounced multiple-front phenotypes in single versus double (mDia1/3) KO cells. Scale bar, 10 μ m. (D) Quantification of protrusive fronts (one versus multiple) from images as shown in C. Error bars, s.e.m. from at least six independent experiments, n, cell number. (E) Quantification of random migration of respective cell types on laminin. Boxes include 50% and whiskers 80% of all measurements, dots represent the 5th/95th percentile. n.s. non-significant, ** p<0.01, *** p<0.001 by Mann-Whitney rank sum test. n, number of tracked cells.

visualize the lipid gradient between front and rear in polarized *Dictyostelium* cells. In highly polarized WT cells, the bulk of F-actin was concentrated in the leading edge and contained only

749
750
751
752
753
754
755
756
757
758
759
760
761
762
763
764
765
766
767
768
769
770
771
772
773
774
775
776
777
778
779
780
781
782
783
784
785
786
787
788
789
790
791
792
793
794
795
796
797
798
799
800
801
802
803
804
805
806
807
808
809
810
811
812
813
814
815
816

817 small amounts of Ctx, while the rear and lateral sides, encom- 885
818 passing the thin layer of cortical actin, were strongly enriched 886
819 for Ctx (Fig. 4C). By contrast, *forA*⁻/*E*⁻/*H*⁻ and *racE*⁻ mutants 887
820 were rounder overall and did not show the characteristic Ctx 888
821 differential. Most notably, large sections of the cortex in both 889
822 mutants were devoid of the cortical actin layer, while remaining 890
823 segments of the cortex still contained prominent F-actin assem- 891
824 blies. Quantification of phalloidin fluorescence intensities across 892
825 the cortex in actin-deficient areas confirmed this view (Fig. 4D), 893
826 and was further substantiated by time-lapse imaging of WT and 894
827 mutant cells expressing the F-actin probe LimEΔcoil-GFP ("SI 895
828 Appendix, Movie S3"). We hypothesized that the thin layer that is 896
829 missing in the mutants corresponds to the contractile actin cortex, 897
830 whereas the remaining and prominent F-actin assemblies repre- 898
831 sent Arp2/3 complex-driven F-actin structures such as leading 899
832 edges or endocytic cups. Thus, we labelled WT and mutant cells 900
833 with phalloidin and for the F-actin binding protein coronin, which 901
834 is a central constituent of Arp2/3 complex-mediated F-actin net- 902
835 works (41). Consistent with the key function of Arp2/3 complex 903
836 in protrusion, coronin was strongly enriched in the leading edges 904
837 of WT cells (Fig. 4E). Notably, coronin was depleted from actin- 905
838 deficient regions, but co-localizing with the prominent F-actin 906
839 assemblies in *forA*⁻/*E*⁻/*H*⁻ and *racE*⁻ mutants, strongly suggesting 907
840 that these structures are nucleated by Arp2/3 complex. Finally, 908
841 we explored the ultrastructural cortex architecture by scanning 909
842 electron microscopy (SEM) after detergent extraction of cells. As 910
843 opposed to the dense, cortical meshwork of WT cells with numer- 911
844 ous overlapping filaments, elimination of the three formins or of 912
845 RacE caused marked differences in cortical actin organization, 913
846 including a lower filament density interspaced with large gaps 914
847 containing much fewer filaments with different geometry (Fig. 915
848 4F).

849 **Cortical formins are essential for motility in 2D-** 916
850 **confinement.** Loss of ForA was previously shown to affect 917
851 cell migration in unconfined and 2D-confined scenarios (17). 918
852 Thus, we analyzed random cell migration of freely moving and 919
853 2D-confined *forA*⁻/*E*⁻/*H*⁻ and *racE*⁻ mutants in phosphate buffer 920
854 (PB) employing phase-contrast time-lapse microscopy, and 921
855 compared migration rates of the mutants to that of WT cells. 922
856 Additionally, we also determined mean square displacement 923
857 (MSD) to discriminate locally restricted movement or wiggling of 924
858 cells from effective directional cell migration (42). Intriguingly, 925
859 elimination of ForA, ForE and ForH or of RacE even increased 926
860 the speed of randomly migrating, mutant cells in unconfined 927
861 environments to $8.2 \pm 2.1 \mu\text{m}\cdot\text{min}^{-1}$ (*forA*⁻/*E*⁻/*H*⁻) or 8.9 ± 2.1 928
862 $\mu\text{m}\cdot\text{min}^{-1}$ (*racE*⁻) (mean±s.d.) as compared to WT controls 929
863 with $6.8 \pm 1.8 \mu\text{m}\cdot\text{min}^{-1}$ (Fig. 5 A and B). However, when 930
864 compressed under a sheet of agar, *forA*⁻/*E*⁻/*H*⁻ and *racE*⁻ mutants 931
865 were abrogated for migration ($1.9 \pm 0.59 \mu\text{m}\cdot\text{min}^{-1}$ and $1.8 \pm$ 932
866 $0.4 \mu\text{m}\cdot\text{min}^{-1}$), as assessed by tracking of the centroids when 933
867 compared to WT ($4.8 \pm 1.9 \mu\text{m}\cdot\text{min}^{-1}$) (Fig. 5 C and D). 934
868 Consistent with their higher motility in unconfined settings, a 935
869 large proportion of both mutants cells were more directional 936
870 and had higher MSD values as compared to control (Fig. 5 E). 937
871 In marked contrast, the MSD values of both mutants virtually 938
872 dropped to zero in 2D-confinement, illustrating their inability 939
873 to migrate under agar, whereas WT cells were still able to 940
874 efficiently migrate under these conditions (Fig. 5F). These 941
875 findings substantiate the fundamental role of the contractile 942
876 actin cortex for cell migration in confinement. 943

877 **Mutants lacking cortical formins or RacE form multiple** 944
878 **fronts.** Amoeboid cells such as *Dictyostelium* cells generally 945
879 exhibit only weak adhesion to the substrate to allow for fast mi- 946
880 gration in unconfined settings. In *Dictyostelium* cells impaired in 947
881 the cortical actin cytoskeleton, cell behavior or establishment and 948
882 maintenance of cell shape are expected to be stronger affected by 949
883 membrane tension. To test this hypothesis, we imaged freely mov- 950
884

ing *forA*⁻/*E*⁻/*H*⁻ and *racE*⁻ mutants at high magnification by time- 885
lapse phase contrast microscopy, and compared their activities to 886
those of WT cells. WT cells were more spherical and typically 887
formed one or two protruding fronts in the form of pseudopods 888
or macropinosomes at a given time. By contrast, *forA*⁻/*E*⁻/*H*⁻ and 889
racE⁻ mutants were considerably flatter, as evidenced by strongly 890
reduced halos in phase-contrast images at their cell boundaries. 891
Notably, about 33% of *forA*⁻/*E*⁻/*H*⁻ cells and 19% of *racE*⁻ cells in- 892
termittently exhibited a fan-shaped, keratocyte-like morphology 893
and migrated with high, directional persistence, which was con- 894
trasted by only 6% of highly directional WT cells ("SI Appendix, 895
Movie S4"). Remarkably, both mutants often developed multiple 896
fronts exhibiting 5 or 6 lamellipodia-like pseudopods (Fig. 6 A 897
and B and "SI Appendix, Movie S5"). The elimination of formins 898
and of RacE also substantially increased the combined protrusion 899
area relative to total cell area in the mutants by more than 30% 900
to $32.0 \pm 5.7\%$ (*forA*⁻/*E*⁻/*H*⁻) and $29.2 \pm 2.0\%$ (*racE*⁻) as compared 901
to WT control ($19.6 \pm 1.7\%$, Fig. 6C). Moreover, the protrusion 902
speed of the fronts in the mutants was about doubled to $0.19 \pm$ 903
 $0.03 \mu\text{m}\cdot\text{sec}^{-1}$ (*forA*⁻/*E*⁻/*H*⁻) and $0.20 \pm 0.03 \mu\text{m}\cdot\text{sec}^{-1}$ (*racE*⁻) when 904
compared to WT control ($0.10 \pm 0.02 \mu\text{m}\cdot\text{sec}^{-1}$) (Fig. 6D). Inter- 905
estingly, inhibition of myosin II by blebbistatin had little effect on 906
the motility of *ForA*⁻/*E*⁻/*H*⁻ and *racE*⁻ mutant cells ("SI Appendix, 907
Fig. S7"), excluding augmented actomyosin contractility as direct 908
cause for these effects. Although RICH analyses revealed a larger 909
contact area of mutant cells ("SI Appendix, Fig. S8 A and B"), 910
they formed fewer actin foci, and these adhesion points were 911
significantly shorter lived than those in controls ("SI Appendix, 912
Fig. S8 C-E"). In line with these observations, the contact area 913
of multiple front- or keratocyte-shaped cells was inhomogeneous 914
and interspersed with less adhesive sections, as evidenced by 915
RICH ("SI Appendix, Movies S6 and S7"). Thus, the combination 916
of increased protrusive activity and decreased adhesiveness in the 917
mutants may explain the highly directional persistence in motility 918
assays. Finally, we noticed that the growth of initially formed 919
fronts in the mutants typically ceased when multiple, competing 920
protrusions were formed on the opposite side of the cell. In these 921
cases, initial fronts rapidly lost adhesion to the underlying surface 922
and were effectively retracted into the cell body ("SI Appendix, 923
Fig. S9 and Movies S 6 and S8"). 924

925 **Polarity defects and dramatically increased cortical actin** 926
927 **flow in *forA*⁻/*E*⁻/*H*⁻ and *racE*⁻ mutants.** An intact contractile 928
actin cortex of amoeboid cells regulates cell migration in 2D- 929
confinement by guiding hydrostatic pressure, created by acto- 930
myosin contraction in the rear, to the front to promote leading 931
edge protrusion (17). Thus, we monitored myosin II and F-actin 932
representing the two main components of the contractile machin- 933
ery in WT and mutant cells after mechanical stress in confinement 934
under agar. WT cells expressing fluorescently-tagged heavy chain 935
of myosin II were highly polarized, and the motor protein was 936
continuously concentrated in a compact, crescent-like sheet at 937
the rear cortex beneath the plasma membrane (Fig. 7A and 938
"SI Appendix, Movie S9"). In striking contrast, *forA*⁻/*E*⁻/*H*⁻ and 939
racE⁻ mutants remained highly unpolarized in 2D-confinement, 940
as evidenced by the aberrant circular localization of myosin II in 941
a band-like fashion along most of the cell periphery, albeit this 942
phenotype was slightly less prominent in *racE*⁻ cells (Fig. 7A). 943
Moreover, myosin II did not accumulate in a crisp band as in 944
WT cells, but was dispersed into multiple, string-like assemblies 945
in the mutants. Myosin II was also largely dislodged from the 946
membrane and was instead strongly enriched at an endoplasm- 947
ectoplasm interface separating the organelle free area from the 948
cell interior (Fig. 7A). Consistently, time-lapse imaging of the 949
mutant cells revealed a highly erratic behavior of myosin II as- 950
sociated with intense blebbing, substantiating the massive defects 951
in the contractile cell cortex of mutant cells ("SI Appendix, Movie 952
S9"). Quantification of myosin II band width as well as its radial

distribution in WT and mutant cells in polarity plots corroborated this view (Fig. 7B).

We then analyzed the dynamic behavior of cortical actin filaments at the ventral plasma membrane by total internal reflection fluorescence (TIRF) microscopy in WT and mutant cells after confinement under agar. In WT cells, cortical actin, visualized by the F-actin marker LimE Δ coil-GFP, was organized into a delicate, filamentous web, interspaced with dynamic actin foci, which accumulated most strongly in protruding fronts evidently driven by Arp2/3 complex-mediated actin assembly (Fig. 7C and ("SI Appendix, Movie S10")). A filamentous network was also observed in the *forA*⁻/*E*⁻/*H*⁻ and *racE*⁻ mutants. However, presumably due to the high membrane tension and their strong polarization defect in 2D-confinement, they did not form protruding fronts. Moreover, as assessed from TIRF time-lapse imaging, the dynamics of cortical actin filaments was drastically changed as compared to control. These filaments were rapidly pulled into the cell center in a process reminiscent of actin retrograde flow in higher eukaryotes. Particle image velocimetry (PIV)-based quantification of cortical actin flow confirmed this notion (Fig. 7D). The velocity distribution showed flows of up to 72 $\mu\text{m}\cdot\text{min}^{-1}$ in *racE*⁻ cells and almost up to 100 $\mu\text{m}\cdot\text{min}^{-1}$ in the *forA*⁻/*E*⁻/*H*⁻ mutant as compared to the average flow with $1.48\pm 1.08 \mu\text{m}\cdot\text{min}^{-1}$ (mean \pm s.d.) in WT cells (Fig. 7E). Consistently, PIV analyses further revealed that the region with fastest actin filament flows overlap with myosin II-enriched regions in *forA*⁻/*E*⁻/*H*⁻ and *racE*⁻ mutants (Fig. 7A and E and ("SI Appendix, Fig. S10")). Together, these data strongly suggest that filaments nucleated by cortical formins regulate subcellular myosin II localization and cortical actin flow under mechanical stress.

Cell lines lacking murine mDia1 and -3 display phenotypes indicative of conserved, cortical functions. To explore whether our observations are generalizable to higher eukaryotes, we analyzed mammalian formins in highly motile B16-F1 mouse melanoma cells. Since mDia subfamily formins (1, 2, and 3) are regulated by RhoA (43), which is well established to drive contractility, we focused on subcellular localization of EGFP-tagged mDia variants after ectopic expression in B16-F1 cells. Consistent with our previous findings (17), we found constitutively active mDia1 variants, i.e. mDia1 Δ DAD as well as the newly designed point mutant mDia1-FL-2xAla (M1182A and F1195A), which is expected to release autoinhibition of the FL protein (44), to localize prominently in the cell rear, whereas the full length, autoinhibited protein remained cytosolic (Fig. 8A). Virtually identical results were obtained with corresponding mDia3 variants (Fig. 8A), whereas active mDia2 was not found in the cell rear, but mostly targeted to filopodia tips (45). To evaluate mDia functions in the mammalian cell cortex, we employed CRISPR/Cas9-mediated disruption of the genes encoding mDia1 and -3, both individually and in combination in B16-F1 cells. Loss of respective protein in independent, clonal cell lines was confirmed by immunoblotting (Fig. 8B). Interestingly, mDia1 levels were evidently increased in both mDia3-KO cell lines, and *vice versa*, indicative of compensatory, regulatory mechanisms presumably serving to sustain sufficient levels of these cortical polarization (Fig. 8B). Phalloidin stainings revealed defects in cell polarization as well as markedly increased frequencies in mDia1 and -3 single mutants of cells forming multiple fronts, a phenotype that was even further increased in mDia1/3 double-KO cells (Fig. 8C and D) and strikingly reminiscent of cortical formin pathway KOs in *Dictyostelium*. Next, we analyzed random cell migration of B16-F1 wildtype and mutant cells on laminin using time-lapse, phase-contrast microscopy. Interestingly, as opposed to *Dictyostelium* cells migrating without 2D-confinement, cell depolarization and apparent stimulation of the multiple front phenotype reduced the efficiency of the highly adhesive mode of melanoma cell migration, likely caused by inefficient protrusion

in a productive, migratory direction. Specifically, whereas single mDia1 and -3 mutants displayed a moderate, but statistically significant reduction of migration rate in this assay (by 11.7%), removal of both mDia1 and -3 decreased migration even further (by 18.4%; Fig. 8E). Together, these data strongly suggest the RhoA-effectors of the mDia formin subfamily, in particular mDia1 and -3 to exert functions in the actin cortex that are conserved in evolution from *Dictyostelium* to mammals.

Discussion

Over thirty years ago, Bray and White postulated that cortical contractility may not only contribute to retraction of the trailing edge, but also to ingression of the cleavage furrow during cytokinesis (46). Since then, localization and participation in both processes has been demonstrated for numerous cell cortex components including myosin II (47), Ctx (27), PTEN (48) and IQGAP family members (28). Here, we demonstrated that three DRFs, ForA, ForE and ForH act synergistically in the assembly of actin filaments in the contractile actin cortex as evidenced by the increasing severity of additive KO phenotypes, which directly correlated with a gradual decrease in mechanical cortex rigidity. We also showed that the active form of the Rho family GTPase RacE, binds to the GBD of ForA, releasing its autoinhibition to initiate actin assembly. RacE shows considerable sequence similarity with Rho proteins from other species and represents the closest homologue of mammalian RhoA in *Dictyostelium* (36, 49). The phenotype of *racE*⁻ cells was similar to that of the triple knockout DRF cells, including large cytokinesis defects in suspension (31) as well as large effects on development (36). This reinforces the idea that the DRFs are required for filament formation, and this is regulated by RacE. Moreover, RacE localizes to the cell rear as well as cleavage furrow in mitotic cells, and is essential for cortical localization of ForA and ForE.

Similar to the redundancy in cortical actin organization exhibited by DRFs in *Dictyostelium*, we also found stronger, complementary phenotypes after combined inactivation of the formins mDia1 and -3 in B16-F1 mouse melanoma cells. This redundancy of the microfilament system is a common phenomenon for essential cellular activities, and has been observed previously for the actin-crosslinking proteins α -actinin and filamin (50) and for Ctx I and II (51) in *Dictyostelium*. While ForA, ForE and ForH act synergistically in actin filament assembly in the contractile actin cortex, it is likely that they also have isoform specific roles and can be activated by other signaling pathways. For example, we found that constitutively active ForH localized to the cortex in unconfined *racE*⁻ cells, but remained largely cytosolic after compression in 2D-confinement, suggesting multiple interactors mediate its subcellular targeting. Of these, RacE is presumably important for ForH targeting under mechanical stress. Incidentally, ForH was recently also found as potential RacE interactor by mass spectrometry (52). In addition, active ForH and ForE also trigger filopodia formation, but as both cortex and filopodia constitute F-actin structures directly associated with the plasma membrane, these actin assembly factors may well participate in the formation of various membrane-associated structures entailing long, unbranched filaments.

The strong effects on cytokinesis and cortex-dependent functions in *forA*⁻/*E*⁻/*H*⁻ are similar to those found in *racE*⁻ cells. This indicates the phenotypic effect of *racE* gene elimination to derive from the lack of *forA/E/H* activation. Consistent with this, none of wild type formins (ForA, ForE or ForH) localized to the cortex as they are likely autoinhibited ("SI Appendix, Fig. S11") and (17). We also found that active RacE accumulates in the cleavage furrow of mitotic cells upon 2D-confinement, implying that it plays a role in regulating cytokinesis by recruitment and activation of cortical formins at this site.

Both *forA*⁻/*E*⁻/*H*⁻ and *racE*⁻ mutants displayed flat morphologies and formation of multiple, dynamic multi-directional protrusions along the cell contour. In agreement with recent work analyzing enhanced expansion of lamellipodial networks upon reduction of plasma membrane load (2), and considering theoretical calculations of cortex mechanics (53), these data imply that cells harboring a compromised viscoelastic cell cortex may experience reduced resistance to actin polymerization forces in protrusions. If correct, this could well cause the formation of amplified protrusions and multiple fronts observed in our mutants. Multiple protrusion formation in *Dictyostelium* was accompanied by adhesion weakening and irregular detachment. Consequently, most unconfined *forA*⁻/*E*⁻/*H*⁻ and *racE*⁻ cells, in some instances resembling fan-shaped keratocytes, migrated faster and more directional than their wildtype controls. These phenotypes appeared at the expense of the more amoeboid type of migration usually seen in *Dictyostelium*.

Of note, the inhibition of myosin II by blebbistatin had little effect on the motility of keratocytes (54) as well as *ForA*⁻/*E*⁻/*H*⁻ and *racE*⁻ mutant cells ("SI Appendix, Fig. S7"). This indicates that the migratory modes adopted by these cell types and/or experimental conditions are less dependent on cortical contractility than during amoeboid or canonical, mesenchymal migration, and additionally mostly driven by the amplified network expansion activity at the leading edges of these cells (55). Interestingly, the migratory behavior of *Dictyostelium* cells can be switched from amoeboid to keratocyte-like by either decreasing PIP2 levels or increasing Ras/Rap signaling (56). Whether or not these phenotypes could relate to the molecular mechanisms described here will be an exciting topic of future study.

In 2-D confinement, *forA*⁻/*E*⁻/*H*⁻ and *racE*⁻ mutants are unable to localize myosin II properly to the cell cortex, polarize and migrate. Symmetry breaking obtained by an anisotropic distribution of components including myosin II drives both, rear retraction in directed cell migration and cytokinesis. How myosin II is localized to the cell cortex is still not fully understood, but has been proposed to include signaling and mechanical cues including myosin phosphorylation by MHCK-A, PTEN, Ctx I or talin in *Dictyostelium* (14, 48, 57, 58) or preferential binding to stretched actin filaments (59). In any case, a severely perturbed cortical actin cytoskeleton will likely interfere with myosin II positioning and activity through all these pathways. Our findings thus establish cortical formins as key to the establishment of polarity and properly regulated migration in both *Dictyostelium* and mammalian cells.

Consistent with the elimination of these formins or their activator RacE, SEM and live-cell TIRF imaging revealed cortical filament density in *forA*⁻/*E*⁻/*H*⁻ and *racE*⁻ cells to be reduced compared to WT, but raised the question as to which assembly factors are involved in generating the remaining cortical actin filaments. Our immunofluorescence results with fixed cells indicated these filaments to be primarily nucleated by remaining prominent actin assembly factors, such as Arp2/3 complex and VASP, although we cannot exclude at this stage the presence of

filaments assembled by other formins, for instance ForG, known to cooperate with Arp2/3 complex in large scale endocytosis (23) or of ForF (dDia1), which homogeneously accumulates in the entire pseudopod (60).

In 2-D confinement, *forA*⁻/*E*⁻/*H*⁻ and *racE*⁻ mutants exhibited exceptionally fast centripetal flows of residual cortical filaments at velocities of 50-100 $\mu\text{m}/\text{min}$, which were contrasted by almost immobile cortical networks relative to the advancement of migrating, wildtype cells. This suggests that in 2D-confinement, *Dictyostelium* does not primarily use retrograde actin fluxes to drive force transmission during migration, as recently proposed for other cell types utilizing amoeboid motility (61, 62). However, the precise cause of the excessive cortical actin flows observed in the mutants remains to be clarified. An intact cortical cytoskeleton harbors various transmembrane proteins and receptors, potentially acting as barriers constraining lateral diffusion (63). Thus, we speculate that the increased cortical flows observed in our mutants are caused by diminished viscosities of their perturbed cortical networks.

Our initial characterization of genome-edited B16-F1 mouse melanoma mutants devoid of mDia1, mDia3 or both formins revealed striking similarities to the *Dictyostelium* system. Comparable to *Dictyostelium* ForA, ForE and ForH, both mammalian formins are regulated by Rho-subfamily proteins, which are ultimately linked to contractility. Active variants of mDia1 and -3, but not the autoinhibited full-length proteins localized prominently to the rear cortex in polarized B16-F1 cells, and the individual elimination of these formins triggered the formation of multiple protrusive fronts as well as substantial defects in polarization and migration. The fact that the phenotypes were noticeably amplified in double mutants reinforced the conclusion of their overlapping functions. This is consistent with a very recent study analyzing the contractile actin cortex in Sertoli cells of mouse seminiferous tubules (64). Loss of mDia1 and -3 in these cells compromised the cortical actin cytoskeleton leading to less dense F-actin meshworks ultimately resulting in impaired spermatogenesis. Taken together, our results suggest that formins are important in cell cortex establishment and maintenance, and that these functions are evolutionarily conserved across far distant organisms.

Materials and Methods

A complete description of the methods is provided in SI Materials and Methods. This description includes construct generation, cell culture, transfections and establishment of *Dictyostelium* and B16-F1 mutants, protein purification, actin-assembly and pull-down assays, antibodies and immunoblots, imaging, aspiration assays, analyses of cell migration, Y2H assays, and quantification of actin flows and statistical analyses.

Acknowledgements

We thank Annette Breskott for technical assistance and all members of the group for inspiring discussions. We further thank Martin Fuller for help with critical point drying and Stuart Micklethwaite and John Harrington of LEMAS (Leeds Electron Microscopy and Spectroscopy Centre) for help with collecting SEM images. This work was supported by Wellcome Trust to M.P. (094231/Z/10/Z), intramural funding from the Helmholtz Society to R.M. and K.R., and the Deutsche Forschungsgemeinschaft to K.R. (GRK2223/1) and J.F. (FA 330/12-1).

1. Blanchoin L, Boujemaa-Paterski R, Sykes C, Plastino J (2014) Actin dynamics, architecture, and mechanics in cell motility. *Physiol Rev* 94(1):235–63.
2. Mueller J, et al. (2017) Load Adaptation of Lamellipodial Actin Networks. *Cell* 171(1):188–200.e16.
3. Kage F, et al. (2017) FMNL formins boost lamellipodial force generation. *Nat Commun* 8. doi:10.1038/ncomms14832.
4. Sackmann E (2015) How actin/myosin crosstalks guide the adhesion, locomotion and polarization of cells. *Biochim Biophys Acta* 1853(11 Pt B):3132–42.
5. Paluch EK, Aspalter IM, Sixt M (2016) Focal Adhesion-Independent Cell Migration. *Annu Rev Cell Dev Biol* 32(1):469–490.
6. Bear JE, Haugh JM (2014) Directed migration of mesenchymal cells: where signaling and the cytoskeleton meet. *Curr Opin Cell Biol* 30:74–82.
7. Charras GT, Coughlin M, Mitchison TJ, Mahadevan L (2008) Life and Times of a Cellular Bleb. *Biophys J* 94(5):1836–1853.
8. Yoshida K, Soldati T (2006) Dissection of amoeboid movement into two mechanically distinct

modes. *J Cell Sci* 119(18):3833–3844.

9. Clark AG, Wartlick O, Salbreux G, Paluch EK (2014) Stresses at the cell surface during animal cell morphogenesis. *Curr Biol* 24(10):R484–94.
10. Chugh P, et al. (2017) Actin cortex architecture regulates cell surface tension. *Nat Cell Biol* 19(6):689–697.
11. Fehon RG, McClatchey AI, Bretscher A (2010) Organizing the cell cortex: the role of ERM proteins. *Nat Rev Mol Cell Biol* 11(4):276–287.
12. Maniti O, et al. (2012) Binding of moesin and ezrin to membranes containing phosphatidylinositol (4,5) biphosphate: A comparative study of the affinity constants and conformational changes. *Biochim Biophys Acta - Biomembr* 1818(11):2839–2849.
13. Stock A, et al. (1999) Domain analysis of cortexillin I: Actin-bundling, PIP2-binding and the rescue of cytokinesis. *EMBO J* 18(19). doi:10.1093/emboj/18.19.5274.
14. Ren Y, et al. (2009) Mechanosensing through Cooperative Interactions between Myosin II and the Actin Crosslinker Cortexillin I. *Curr Biol* 19(17):1421–1428.
15. Kee Y-S, et al. (2012) A mechanosensory system governs myosin II accumulation in dividing

- 1225 cells. *Mol Biol Cell* 23(8):1510–23.
- 1226 16. Salbreux G, Charras G, Paluch E (2012) Actin cortex mechanics and cellular morphogenesis. *Trends Cell Biol* 22(10):536–545.
- 1227 17. Ramalingam N, et al. (2015) A resilient formin-derived cortical actin meshwork in the rear drives actomyosin-based motility in 2D confinement. *Nat Commun* 6. doi:10.1038/ncomms9-496.
- 1228 18. Rottner K, Faix J, Bogdan S, Linder S, Kerkhoff E (2017) Actin assembly mechanisms at a glance. *J Cell Sci* 130(20). doi:10.1242/jcs.206433.
- 1229 19. Pollard TD (2007) Regulation of Actin Filament Assembly by Arp2/3 Complex and Formins. *Annu Rev Biophys Biomol Struct* 36(1):451–477.
- 1230 20. Kühn S, Geyer M (2014) Formins as effector proteins of Rho GTPases. *Small GTPases* 5(3):e983876.
- 1231 21. Lammers M, Rose R, Scrima A, Wittinghofer A (2005) The regulation of mDia1 by autoinhibition and its release by Rho*GTP. *EMBO J* 24(23):4176–87.
- 1232 22. Li F, Higgs HN (2005) Dissecting Requirements for Auto-inhibition of Actin Nucleation by the Formin, mDia1. *J Biol Chem* 280(8):6986–6992.
- 1233 23. Junemann A, et al. (2016) A Diaphanous-related formin links Ras signaling directly to actin assembly in macropinocytosis and phagocytosis. *Proc Natl Acad Sci* 113(47):E7464–E7473.
- 1234 24. Bovellan M, et al. (2014) Cellular Control of Cortical Actin Nucleation. *Curr Biol* 24(14):1628–1635.
- 1235 25. Fritzsche M, Erlenkämper C, Moeendarbary E, Charras G, Kruse K (2016) Actin kinetics shapes cortical network structure and mechanics. *Sci Adv* 2(4):e1501337.
- 1236 26. Fukui Y, Inoué S (1991) Cell division in *Dictyostelium* with special emphasis on actomyosin organization in cytokinesis. *Cell Motil Cytoskeleton* 18(1):41–54.
- 1237 27. Weber I, et al. (1999) Cytokinesis mediated through the recruitment of cortexillins into the cleavage furrow. *EMBO J* 18(3):586–594.
- 1238 28. Faix J, et al. (2001) Recruitment of cortexillin into the cleavage furrow is controlled by Rac1 and IQGAP-related proteins. *EMBO J* 20(14):3705–15.
- 1239 29. Bohnert KA, Willet AH, Kovar DR, Gould KL (2013) Formin-based control of the actin cytoskeleton during cytokinesis. *Biochem Soc Trans* 41(6). Available at: <http://www.biochemsoctrans.org/content/41/6/1750.long> [Accessed May 25, 2018].
- 1240 30. Rivero F, Dislich H, Glöckner G, Noegel AA (2001) The Dictyostelium discoideum family of Rho-related proteins. *Nucleic Acids Res* 29(5):1068–79.
- 1241 31. Gerald N, Dai J, Ting-Beall HP, De Lozanne A (1998) A role for Dictyostelium racE in cortical tension and cleavage furrow progression. *J Cell Biol* 141(2):483–92.
- 1242 32. Laroche DA, Vithalani KK, De Lozanne A (1997) Role of Dictyostelium racE in cytokinesis: mutational analysis and localization studies by use of green fluorescent protein. *Mol Biol Cell* 8(5):935–44.
- 1243 33. Rivero F, et al. (2005) A comparative sequence analysis reveals a common GBD/FH3-FH1-FH2-DAD architecture in formins from Dictyostelium, fungi and metazoa. *BMC Genomics* 6(1):28.
- 1244 34. Muramoto T, Urushihara H (2006) Small GTPase RacF2 affects sexual cell fusion and asexual development in Dictyostelium discoideum through the regulation of cell adhesion. *Dev Growth Differ* 48(3):199–208.
- 1245 35. Schreienbeck A, Bretschneider T, Arasada R, Schleicher M, Faix J (2005) The Diaphanous-related formin dDia2 is required for the formation and maintenance of filopodia. *Nat Cell Biol* 7(6). doi:10.1038/ncb1266.
- 1246 36. Wang Y, Senoo H, Sesaki H, Iijima M (2013) Rho GTPases orient directional sensing in chemotaxis. *Proc Natl Acad Sci* 110(49):E4723–E4732.
- 1247 37. Chen P, Ostrow BD, Tafuri SR, Chisholm RL (1994) Targeted disruption of the Dictyostelium RMLC gene produces cells defective in cytokinesis and development. *J Cell Biol* 127(6). Available at: <http://jcb.rupress.org/content/127/6/1933.long> [Accessed May 25, 2018].
- 1248 38. Laroche DA, Vithalani KK, De Lozanne A (1996) A novel member of the rho family of small GTP-binding proteins is specifically required for cytokinesis. *J Cell Biol* 133(6):1321–9.
- 1249 39. Springer ML, Patterson B, Spudich JA (1994) Stage-specific requirement for myosin II during Dictyostelium development. *Development* 120(9):2651–60.
- 1250 40. Shu S, Liu X, Kriebel PW, Daniels MP, Korn ED (2012) Actin cross-linking proteins cortexillin I and II are required for cAMP signaling during Dictyostelium chemotaxis and development. *Mol Biol Cell* 23(2):390–400.
- 1251 41. Bretschneider T, et al. (2002) Dynamic organization of the actin system in the motile cells of Dictyostelium. *J Muscle Res Cell Motil* 23(7–8):639–49.
- 1252 42. Litschko C, et al. (2017) Differential functions of WAVE regulatory complex subunits in the regulation of actin-driven processes. *Eur J Cell Biol*. doi:10.1016/j.ejcb.2017.08.003.
- 1253 43. Lammers M, Meyer S, Kühlmann D, Wittinghofer A (2008) Specificity of Interactions between mDia Isoforms and Rho Proteins. *J Biol Chem* 283(50):35236–35246.
- 1254 44. Lammers M, Rose R, Scrima A, Wittinghofer A (2005) The regulation of mDia1 by autoinhibition and its release by Rho*GTP. *EMBO J* 24(23):4176–4187.
- 1255 45. Block J, et al. (2008) Filopodia formation induced by active mDia2/Drf3. *J Microsc* 231(3). doi:10.1111/j.1365-2818.2008.02063.x.
- 1256 46. Bray D, White JG (1988) Cortical flow in animal cells. *Science* 239(4842):883–8.
- 1257 47. Moores SL, Sabry JH, Spudich JA (1996) Myosin dynamics in live Dictyostelium cells. *Proc Natl Acad Sci U S A* 93(1):443–6.
- 1258 48. Pramanik MK, Iijima M, Iwadate Y, Yumura S (2009) PTEN is a mechanosensing signal transducer for myosin II localization in Dictyostelium cells. *Genes Cells* 14(7):821–34.
- 1259 49. Vlahou G, Rivero F (2006) Rho GTPase signaling in Dictyostelium discoideum: Insights from the genome. *Eur J Cell Biol* 85(9–10):947–959.
- 1260 50. Witke W, Schleicher M, Noegel AA (1992) Redundancy in the microfilament system: abnormal development of Dictyostelium cells lacking two F-actin cross-linking proteins. *Cell* 68(1):53–62.
- 1261 51. Faix J, et al. (1996) Cortexillins, major determinants of cell shape and size, are actin-bundling proteins with a parallel coiled-coil tail. *Cell* 86(4). doi:10.1016/S0092-8674(00)80136-1.
- 1262 52. Senoo H, Cai H, Wang Y, Sesaki H, Iijima M (2016) The novel RacE-binding protein GflB sharpens Ras activity at the leading edge of migrating cells. *Mol Biol Cell* 27(10):1596–605.
- 1263 53. Sens P, Plastino J (2015) Membrane tension and cytoskeleton organization in cell motility. *J Phys Condens Matter* 27(27):273103.
- 1264 54. Keren K, Yam PT, Kinkhabwala A, Mogilner A, Theriot JA (2009) Intracellular fluid flow in rapidly moving cells. *Nat Cell Biol* 11(10):1219–1224.
- 1265 55. Keren K (2011) Cell motility: the integrating role of the plasma membrane. *Eur Biophys J* 40(9):1013–1027.
- 1266 56. Miao Y, et al. (2017) Altering the threshold of an excitable signal transduction network changes cell migratory modes. *Nat Cell Biol* 19(4):329–340.
- 1267 57. Steimle PA, et al. (2001) Recruitment of a myosin heavy chain kinase to actin-rich protrusions in Dictyostelium. *Curr Biol* 11(9):708–13.
- 1268 58. Tsuboi M, et al. (2012) Talin couples the actomyosin cortex to the plasma membrane during rear retraction and cytokinesis. *Proc Natl Acad Sci U S A* 109(32):12992–7.
- 1269 59. Uyeda TQP, Iwadate Y, Umeki N, Nagasaki A, Yumura S (2011) Stretching actin filaments within cells enhances their affinity for the myosin II motor domain. *PLoS One* 6(10):e26200.
- 1270 60. Winterhoff M, et al. (2014) The Diaphanous-related formin dDia1 is required for highly directional phototaxis and formation of properly sized fruiting bodies in Dictyostelium. *Eur J Cell Biol* 93(5–6). doi:10.1016/j.ejcb.2013.11.002.
- 1271 61. Bergert M, et al. (2015) Force transmission during adhesion-independent migration. *Nat Cell Biol* 17(4):524–9.
- 1272 62. Liu Y-J, et al. (2015) Confinement and low adhesion induce fast amoeboid migration of slow mesenchymal cells. *Cell* 160(4):659–672.
- 1273 63. Ostrowski PP, Grinstein S, Freeman SA (2016) Diffusion Barriers, Mechanical Forces, and the Biophysics of Phagocytosis. *Dev Cell* 38(2):135–46.
- 1274 64. Sakamoto S, et al. (2018) mDia1/3 generate cortical F-actin meshwork in Sertoli cells that is continuous with contractile F-actin bundles and indispensable for spermatogenesis and male fertility. *PLoS Biol* 16(9):e2004874.
- 1275 65. Levi S, Polyakov M V, Egelhoff TT (2002) Myosin II dynamics in Dictyostelium: determinants for filament assembly and translocation to the cell cortex during chemoattractant responses. *Cell Motil Cytoskeleton* 53(3):177–88.
- 1276 66. Veltman DM, Keizer-Gunnink I, Haastert PJM Van (2009) An extrachromosomal, inducible expression system for Dictyostelium discoideum. *Plasmid* 61(2):119–125.
- 1277 67. Schneider N, et al. (2003) A Lim protein involved in the progression of cytokinesis and regulation of the mitotic spindle. *Cell Motil Cytoskeleton* 56(2). doi:10.1002/cm.10139.
- 1278 68. Linkner J, Nordholz B, Junemann A, Winterhoff M, Faix J (2012) Highly effective removal of floxed Blasticidin S resistance cassettes from Dictyostelium discoideum mutants by extrachromosomal expression of Cre. *Eur J Cell Biol* 91(2):156–60.
- 1279 69. Ran FA, et al. (2013) Genome engineering using the CRISPR-Cas9 system. *Nat Protoc* 8(11):2281–2308.
- 1280 70. Ramalingam N, et al. (2010) Phospholipids regulate localization and activity of mDia1 formin. *Eur J Cell Biol* 89(10):723–732.
- 1281 71. Spudich JA, Watt S (1971) The regulation of rabbit skeletal muscle contraction. I. Biochemical studies of the interaction of the tropomyosin-troponin complex with actin and the proteolytic fragments of myosin. *J Biol Chem* 246(15):4866–71.
- 1282 72. Troll H, et al. (1992) Purification, functional characterization, and cDNA sequencing of mitochondrial porin from Dictyostelium discoideum. *J Biol Chem* 267(29):21072–9.
- 1283 73. de Hostos EL, Bradtke B, Lottspeich F, Guggenheim R, Gerisch G (1991) Corin, an actin binding protein of Dictyostelium discoideum localized to cell surface projections, has sequence similarities to G protein beta subunits. *EMBO J* 10(13):4097–104.
- 1284 74. Small JV, Rottner K, Hahne P, Anderson KI (1999) Visualising the actin cytoskeleton. *Microsc Res Tech* 47(1):3–17.
- 1285 75. Svitkina TM (2009) Imaging Cytoskeleton Components by Electron Microscopy. *Methods in Molecular Biology (Clifton, N.J.)*, pp 187–206.
- 1286 76. Dielweid S, et al. (2010) Mechanical Properties of Bare and Protein-Coated Giant Unilamellar Phospholipid Vesicles. A Comparative Study of Micropipet Aspiration and Atomic Force Microscopy. *Langmuir* 26(13):11041–11049.
- 1287 77. Schindelin J, et al. (2012) Fiji: an open-source platform for biological-image analysis. *Nat Methods* 9(7):676–682.
- 1288 78. Thielicke W, Stamhuis EJ (2014) PIVlab – Towards User-friendly, Affordable and Accurate Digital Particle Image Velocimetry in MATLAB. *J Open Res Softw* 2. doi:10.5334/jors.bl
- 1289 79. Auferheide KJ, Janetopoulos C (2016) Migration of Dictyostelium discoideum to the Chemoattractant Folic Acid. *Methods in Molecular Biology (Clifton, N.J.)*, pp 25–39.